We are IntechOpen, the world's leading publisher of Open Access books Built by scientists, for scientists

4,800
Open access books available

122,000
International authors and editors

135M
Downloads

Our authors are among the

154
Countries delivered to

TOP 1%
most cited scientists

12.2%
Contributors from top 500 universities

CLARIVATE ANALYTICS BOOK CITATION INDEX INDEXED

WEB OF SCIENCE™

Selection of our books indexed in the Book Citation Index in Web of Science™ Core Collection (BKCI)

Interested in publishing with us?
Contact book.department@intechopen.com

Numbers displayed above are based on latest data collected.
For more information visit www.intechopen.com

Chapter 9

Utilization of Ground-Penetrating Radar and Frequency Domain Electromagnetic for Investigation of Sewage Leaks

Goldshleger Naftaly and Basson Uri

Additional information is available at the end of the chapter

http://dx.doi.org/10.5772/62156

Abstract

Fact 1: Underground sewage pipe systems deteriorate over time, developing cracks and joint defects; therefore, leakage is inevitable. Fact 2: The massive worldwide urbanization process, together with rural development, has meaningfully increased the length of sewage pipelines. Result: The concomitant risk of sewage leaks exposes the surrounding land to potential contamination and environmental harm. It is therefore important to locate such leaks in a timely manner, enabling damage control. Advances in active remote-sensing technologies (GPR and FDEM: ground-penetration radar and frequency domain electromagnetic) were used to identify sewage leaks that might cause pollution and to identify minor spills before they cause widespread damage.

Keywords: Active remote sensing, FDEM, GPR, Sewage leak, Contamination, Water pollution

1. Introduction

Water pollution is the contamination of bodies of water such as aquifers, lakes, ponds, rivers and oceans. This contamination occurs due to direct or indirect discharge of pollutants into the water bodies, without a suitable treatment to remove harmful compounds (pollutants may simply be defined as substances added to the environment that do not belong there). A substantial proportion of water and environmental contaminants are due to leaks from underground sewage pipeline systems in rural, urban and industrial areas, since any sewage pipeline system deteriorates over time, developing cracks and joint defects. Therefore, if sewage pipeline systems are not maintained properly, it is only a matter of time before the sewage leaks out and contaminates the surrounding groundwater and surface water.

Here, we suggest detecting sewage leaks from pipeline systems using two orthogonal active remote-sensing methods: (I) ground-penetrating radar (GPR) and (II) frequency domain electromagnetic (FDEM). Our hypothesis is that GPR and FDEM screening, which creates subsurface images around and along pipeline systems, will enable the extraction of residual signals and the detection of meaningful leaks. Like most complex near-surface detection missions, detection of sewage leaks in an urban environment requires a professional understanding of the regional setting, from geomorphological, environmental and engineering perspectives.

Advances in remote-sensing technologies now enable their use to identify leakage that is potentially responsible for pollution and to identify minor spills before they can cause widespread damage. The detection of pollutants using GPR [1], was based on the research of Basson [2]. Basson [3] presented a combination of GPR and FDEM methods to detect and monitor saline contaminants in agricultural fields. Goldshleger [4, 5] demonstrated the ability to detect saline-affected soils using remote-sensing methods, toward improved management of these soils. Basson [6] described the detection of subsurface water/sewage/drainage pipe systems and leaks/contamination from such pipes. Ben-Dor [7, 8] reviewed remote-sensing–based methods to assess soil salinity and improve the management of salinity-affected soils. Ly and Chui [9] developed accurate representations of weep holes and leaky sewage pipes, and further showed the systems' long-term and short-term responses to rainfall events. Their simulation results provided a better understanding of local-scale migration of sewage leaks from a sewage pipe to nearby storm water drains. The last few years in Israel have seen increasing use of new methods based on active remote-sensing tools to study subsoil quality. These tools include GPR and underground monitoring systems measuring spatial moisture content, such as FDEM in the subsurface. The use of GPR is based on a method that was originally developed for measuring sand dunes of medium moisture content at an unsaturated resolution of a few percentage points [2]. The GPR helped define the possible reason for emerging high-salinity areas, such as a subsurface regional structure that reduces water infiltration into the deeper groundwater position [5]. The FDEM method provided a very important view of salt contamination in the soil layers (except the root zone layer) and also pinpointed areas with salinity problems. The images obtained from FDEM readings provided a subsurface view that also helped identify the reason for the high salinity in certain areas. In the soil salinity experiment in Israel, a severe defect in the drainage pipelines could be observed, which helped the farmers solve the problem before the subsequent season [5].

The present study focuses on the development of these electromagnetic (EM) methods to replace conventional acoustic methods for the identification of sewage pipe leaks. EM methods provide an additional advantage in that they allow mapping the fluid transport system in the subsurface. Leak-detection systems using GPR and FDEM are not limited to large amounts of water, but can also detect leaks of tens of liters per hour, because they can locate increases in pipes' or tanks' environmental moisture content that amount to only a few percentage points. The importance and uniqueness of this research lies in the development of practical tools to provide a snapshot of the spatial changes in soil moisture content to depths of about 3–4 m (in areas with asphalt overlay) at relatively low cost, in real time or close to real time. Spatial

http://dx.doi.org/10.5772/62156

measurements performed using GPR and FDEM systems allow monitoring many tens of thousands of measurement points per hectare, thus providing a picture of the spatial situation along the pipelines. The main purpose of this study was to develop a method for detecting sewage leaks using the above-proposed geophysical methods, as the resultant contaminants can severely affect public health. We focused on identifying, locating and characterizing such leaks in sewage pipes in residential and industrial areas.

2. Methods

In recent years, there has been an increase in the use of active remote-sensing tools, such as GPR (Figure 1a) and subsurface FDEM (Figure 1b), for measuring the subsurface's EM velocity and dielectric constant (GPR), and its electrical conductivity profile and magnetic susceptibility (FDEM).

(a)

(b)

Figure 1. Taking measurements with the RAMAC GPR (a) and Gem-2 FDEM (b) in the study area.

Passive remote-sensing spectroscopy of ground surface and cross-sections using an optical fiber termed SPSP (subsurface-penetrating spectral probe), developed [10] and have been conducted as well. This study focuses on remote-sensing tools to replace acoustic methods [11, 12, 13]. EM methods provide the added advantage of being able to map underground liquid-carrying pipelines. Ground leak-detection systems using GPR and FDEM are not limited to large amounts of water: small leaks of tens of liters per hour can be detected in the environment by comparing medium-dry to minimum moisture content in the pipeline and the canal zone.

Our aim was to develop practical tools that would provide a snapshot of changes in spatial soil moisture content to depths of about 3–4 m in areas covered with asphalt at relatively low cost and in real time. The spatial measurements were performed with FDEM and GPR systems that allow measuring tens of thousands of points per hectare and thus enable monitoring the spatial situation along the pipeline.

2.1. FDEM

Traditionally, the electrical method "measures" apparent resistivity using electrodes that require ground contact in a DC electrical survey, while the EM method "measures" apparent conductivity without ground contact. The EM method, known as a "potential method", involves transmitting and receiving EM fields, commonly using a set of coils. The common unit of resistivity is ohm-m and conductivity is its inverse, in Siemen/m. The apparent resistivity ρ_a is defined in DC resistivity as:

$$\rho_a = 2\pi G \frac{\Delta V}{I} \tag{1}$$

where ΔV is the voltage between a pair of potential electrodes, I is the current that flows through another pair of source electrodes, and G is the geometric factor that depends on the geometry of the electrodes. For a Wenner array that uses four equally spaced electrodes, for instance, G is the electrode spacing itself. Even for this simple array, each electrode spacing generates a different apparent resistivity because the spacing controls the volume of the subsurface sampled by the measurement. It is only when the earth is a homogeneous half space that the apparent resistivity is the same as the true resistivity.

Similarly, apparent conductivity is only same as the true conductivity when the earth is a homogeneous half space. As an example, consider a pair of horizontal coils separated by a distance *r.* A routinely measured quantity is called the *mutual coupling ratio* which, for a horizontal coplanar (or vertical dipole) coil configuration over a layered earth as derived by [14, 15, 16, 17], among others is written as:

$$Q = \frac{H\mathrm{s}}{H\mathrm{p}} = -r^3 \int_0^\infty \lambda^2 R(\lambda) J_0(\lambda r) e^{-\lambda h} d\lambda \tag{2}$$

Hp and Hs are the primary and secondary fields at the receiver coil; $J0$ is the 0th order Bessel function; r is the coil separation and h is the sensor height above the ground. Q represents the

http://dx.doi.org/10.5772/62156

secondary field normalized against the primary field at the receiver coil. Most frequency-domain sensors measure Q in parts per million (ppm). The kernel R corresponding to a homogeneous half space is:

$$R(\lambda) = \frac{\lambda - \sqrt{\lambda^2 + \imath 2\pi f \mu\sigma}}{\lambda + \sqrt{\lambda^2 + \imath 2\pi f \mu\sigma}} \tag{3}$$

where f is the transmitter frequency in Hz, μ the magnetic permeability and σ the half-space conductivity. Based on Q measured at a particular frequency over a real (heterogeneous) earth, we can invert Equation (2) to obtain the *apparent* half-space conductivity σ_a. It is obvious from Equation (2) that the resulting σ depends on coil separation, sensor height and frequency. In addition, each coil configuration (vertical coplanar, coaxial, etc.) has a different formula for Q. Figure 2 shows a coplanar coil pair at height h above layered earth [18], and a damped least-squares inversion based on singular value decomposition to solve the nonlinear inverse problem.

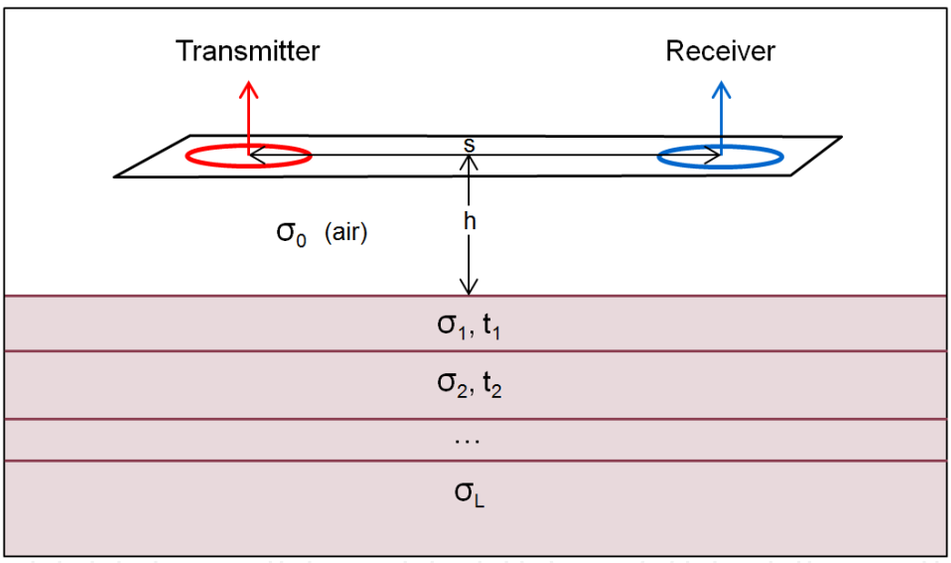

Figure 2. Geometry of the horizontal coplanar electromagnetic sensor over layered earth where σ is the conductivity, t is the thickness of each layer, the subscripts stand for the number of layers, s is the coil separation and h is the sensor height [18].

Figure 3 shows the responses of the Gem-2 sensor over a half space as a function of induction number:

$$\theta = \left(\sigma\mu\omega/2\right)^{1/2} s \tag{4}$$

where ω is the angular frequency, μ is the magnetic permeability and s is coil separation.

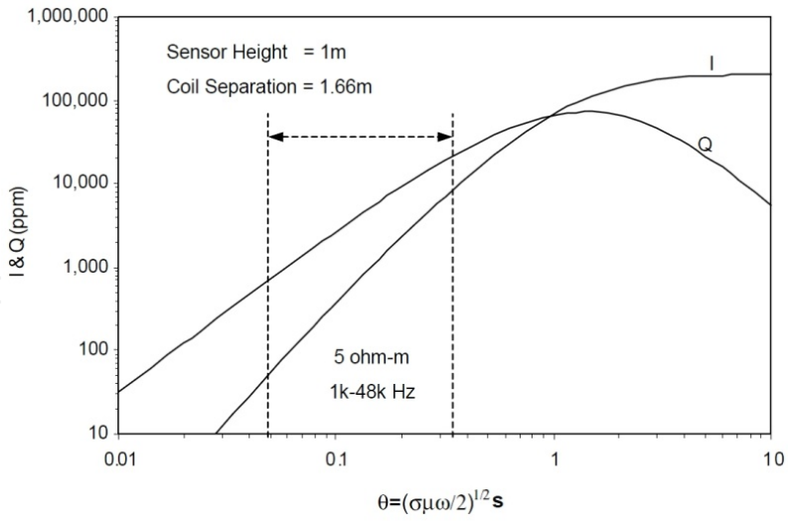

Figure 3. The in-phase and quadrate responses as a function of induction number (from Huang and Won, 2003).

The depth of investigation of an EM system can be estimated using the skin depth δ, which is defined in classical EM theory as the distance in a homogeneous medium over which the amplitude of a plane wave is attenuated by a factor of $1/e$, or about 37% of its original amplitude. The skin depth δ is:

$$\delta = \sqrt{\frac{2}{\sigma\mu\omega}} \tag{5}$$

The skin depth and the ability to transmit in several frequencies allows us to perform "frequency sounding" using a multifrequency sensor, thereby resolving different depths of penetration as sketched in Figure 4.

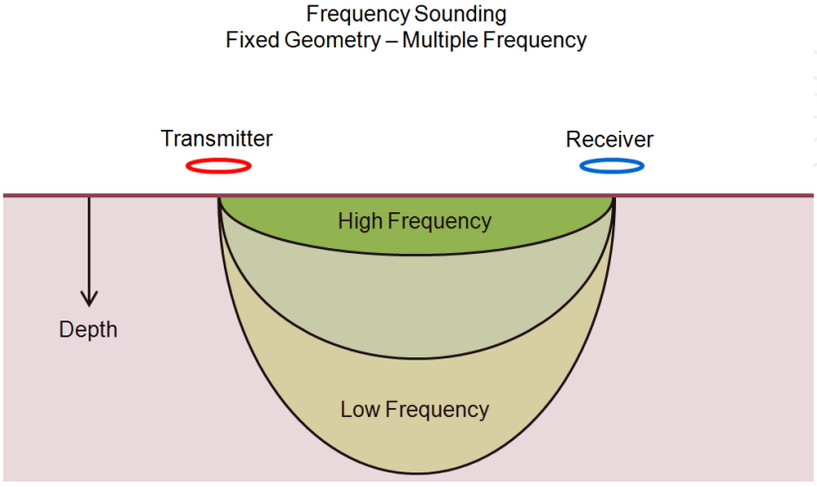

Figure 4. Frequency sounding for various depths using a multifrequency FDEM sensor such as Gem-2.

http://dx.doi.org/10.5772/62156

2.2. GPR

GPR, a reflection-scattering imaging method, is widely used for subsurface imaging in geophysics. GPR uses high frequencies (wavelengths; MHz–GHz). EM waves may form images of the subsurface by transmitting radar pulses into the ground and receiving the deflected waves from the interfaces below. Using wave methods and analysis, GPR images can be analyzed for their derived electrical properties and subsurface characteristics and for spatial mapping of water content [2, 3]. The range resolution is a function of the subsurface dielectric constants and the wave's frequency. It may vary from several centimeters to several tens of centimeters at the relevant effective frequencies [19, 20] For a certain wavelength, the penetration of GPR waves into the subsurface is mainly a function of the host material's conductivity, and therefore GPR waves decay significantly in conductive and saline soils. Using wave methods and analysis, GPR images can be analyzed for their derived electrical properties and subsurface characteristics and for spatial mapping of water content [2,3], as described in the following model.

The connection between the EM velocity and dielectric constant is expressed as:

$$v = \frac{c}{\sqrt{k}} \tag{6}$$

where c is the speed of light in a vacuum and k is the dielectric constant.

The dielectric constant of water (k_w) is about 80. The dielectric constant of air (k_a) is 1. The dielectric constant of common "dry" soil ($k_{\text{dry soil}}$) with residual moisture content can range between 6 and 15 (the effective dielectric constant of dry soil is determined according to volumetric mixing ratios between soil, water and air components).

The difference in the effective dielectric constant of "dry" and "wet" soils is mainly a function of the ratio between the air and water volumes, when the volumes are normalized to:

$$V_{\text{dry soil}} + V_w + V_a = 1 \tag{7}$$

then:

$$k_{\text{eff}} = k_{\text{dry soil}} V_{\text{dry soil}} + k_w V_w + k\left(1 - V_w\right) \tag{8}$$

The maximal soil–water absorbency is a strong function of the effective porosity.

3. Leak detection in Ariel

Ariel is a small city (about 20,000 residents) in Israel, located in the central highland region known as the Samarian Hills. It is situated 40 km (25 miles) east of Tel Aviv and 40 km west

of the Jordan River. It is situated 700 m (more than 2000 feet) above sea level. The city stretches over 12 km (8 miles) in length and 2 km in width. The research was performed with Yuvalim, the company that is responsible for maintaining the water and sewage network in the Ariel area and for supplying available water to residents. The mutual research was performed to identify sewage leaks before they pollute and damage the surrounding area. The research was supported by the Israeli Water Authority. The work was performed in several stages.

3.1. Selecting study sites

Areas were selected in Ariel for system calibration (Figure 5). Two areas were chosen for the method calibration: the first was an industrial area and the second a residential area, both with well-mapped networks of water and sewage pipes. These areas were selected on the basis of information from computerized data, observations, field visits, use of orthophotos, aerial photography and geological and pedological data.

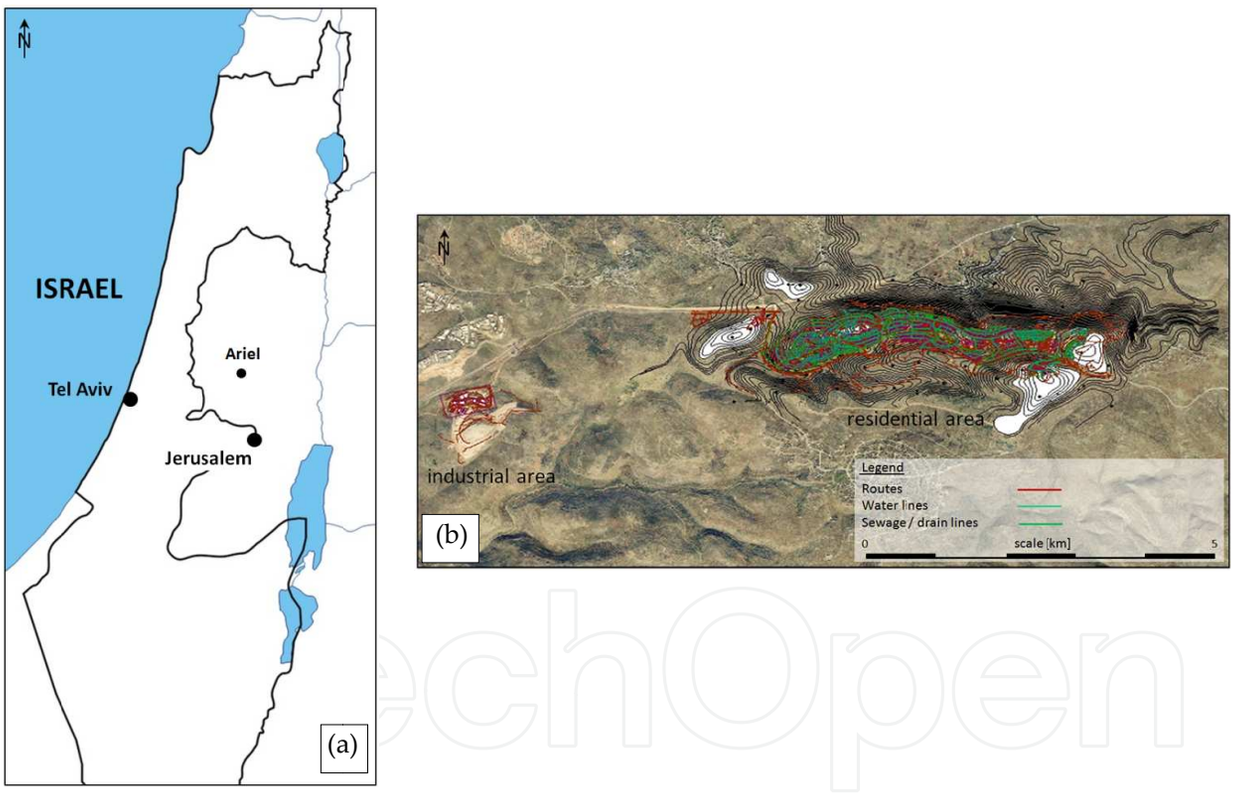

Figure 5. Maps showing Ariel's location (a) and the drainage infrastructure, sewerage and water supply for this city (b).

3.2. Soil characterization

To characterize the pedological structure of the subsurface layers, excavations were performed. We sampled grain size, void content and porosity, moisture content, soil density and soil characteristics. We dug a channel in an underground sewage pipe replacement area at the experimental sites. Figure 6 presents the characterization of the sub layer.

http://dx.doi.org/10.5772/62156

Figure 6. Soil subsurface cross-section at site 1. Wooden pegs mark the changing soil layers.

The soil in the area is red Mediterranean, also known as Terra Rossa [21] and Lithic ruptic Xerochrept [22]. Terra Rossa occurs in areas where heavy rainfall dissolves carbon from the parent calcium carbonate rock and silicates are leached out of the soil, leaving residual deposits that are rich in iron hydroxides, causing the red color. Such areas are usually depressions within limestone. The soil was sampled in a 0.5-m-wide ditch at a depth of 2 m. The area has an easterly aspect, with an average elevation of 400 m above sea level. The local slopes vary between 7% and 25%. Soil texture was clay loam with an average composition of 45% sand, 25% silt and 30% clay. The sand content increased toward the lower part of the area. The average lime content was 30%. Rock fragments of up to 40 cm appeared together with the soil.

3.3. GPR calibration

Calibration of the GPR system to the subsurface properties of the cross-section in a dry state (without leakage) is shown in Figure 7. The depth to the pipe was measured in a nearby manhole.

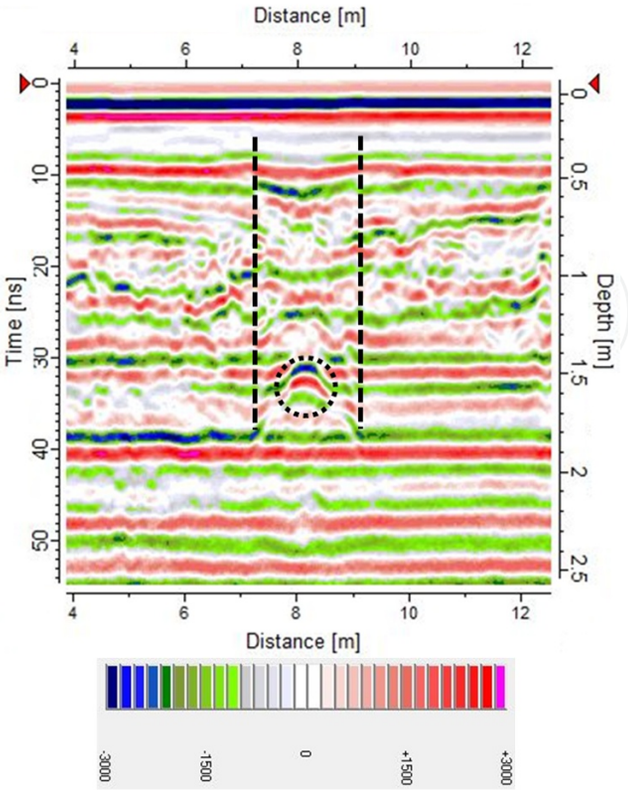

Figure 7. Part of the GPR profile performed for calibration of the GPR system in the Ariel industrial zone, on the road close to a rubber factory. The black circle displays diffraction created by the drain pipe. Above it, the trench is detected as well. The horizontal scale describes the measurement location (in meters) along the profile. The vertical scales describe the time (in nanoseconds) and depth (in meters). The amplitude–intensity scale is shown as well.

Figure 7 shows the results of advanced processing of a cross-section for calibration of the system in the industrial area. On the horizontal scale, simulations are described above the measurement location along the incision in meters; the vertical scales describe the time and depth of the reflections on a timescale of 50 ns and scale depth of 2.5 m below the surface (the strength of the reflections is graded according to the color scale in Figure 7, where the diffraction created by the drainage pipe can be deduced from a return time from the pipe of approximately 32 ns). The diffraction depth is 2.45 m, and the data from the system matches the data measured on the ground. This adaptation makes it possible to determine the velocity of the EM wave. The average measured subsurface speed of the EM wave (v) was 0.093 ± 0.001 m/ns at the Ariel industrial site. It is important to note that the speed of the wave depends on the directly calculated form and location of the anomaly and thus data processing is critical to the research results.

3.4. The experimental site

The experimental site for sewage pipeline and manhole leaks was located near Ariel's old stadium, not far from HaAtsmaut Street (Figure 8, blue rectangle), where a project for the replacement of old sewer pipes has been initiated.

http://dx.doi.org/10.5772/62156

Figure 8. The experimental site is located at the western end of the sewage line adjacent to HaAtsmaut Street (blue rectangle). It includes 12-in. diameter iron pipes carrying on the order of 1000–1200 m^3 sewage water per day, and an average 100 m^3/h during peak flow.

Leakage was initiated in two places at the western site by cracking the sewer pipes close to their bottom side. One crack was made about 6 m from the sewage pit in the northern iron pipe using an electrical disk that created a wedge-shaped hole 15–20 cm in diameter; the second crack was also a circle of 15–20 cm diameter in the lower part of the pipe (Figure 9). The experimental site was monitored daily by radar and FDEM before the start of and during the controlled leakage.

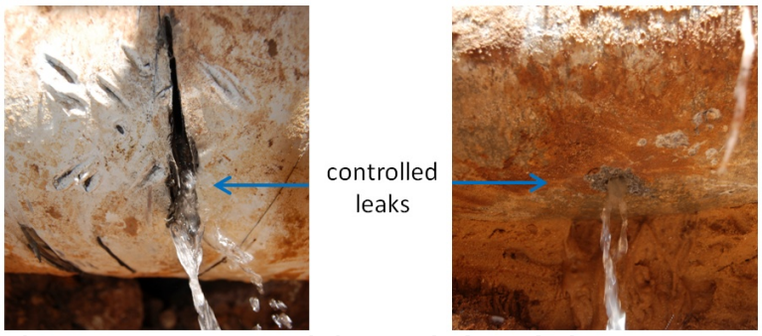

Figure 9. Pictures of the two cracks made in the sewer pipes for the controlled leakage experiment.

4. Results

Daily monitoring with the FDEM method included five cross-sections: four were parallel to the sewer pipeline and the fifth was above it, running on each side of the pipeline at a distance of 0.5 m. During the experiment, FDEM scanning was performed to qualify the effect of moisture on the soil cross-section. Figure 10 shows the status of the subsurface before the start of the controlled leak; it was in a relatively dry state characteristic of the month of May at this site.

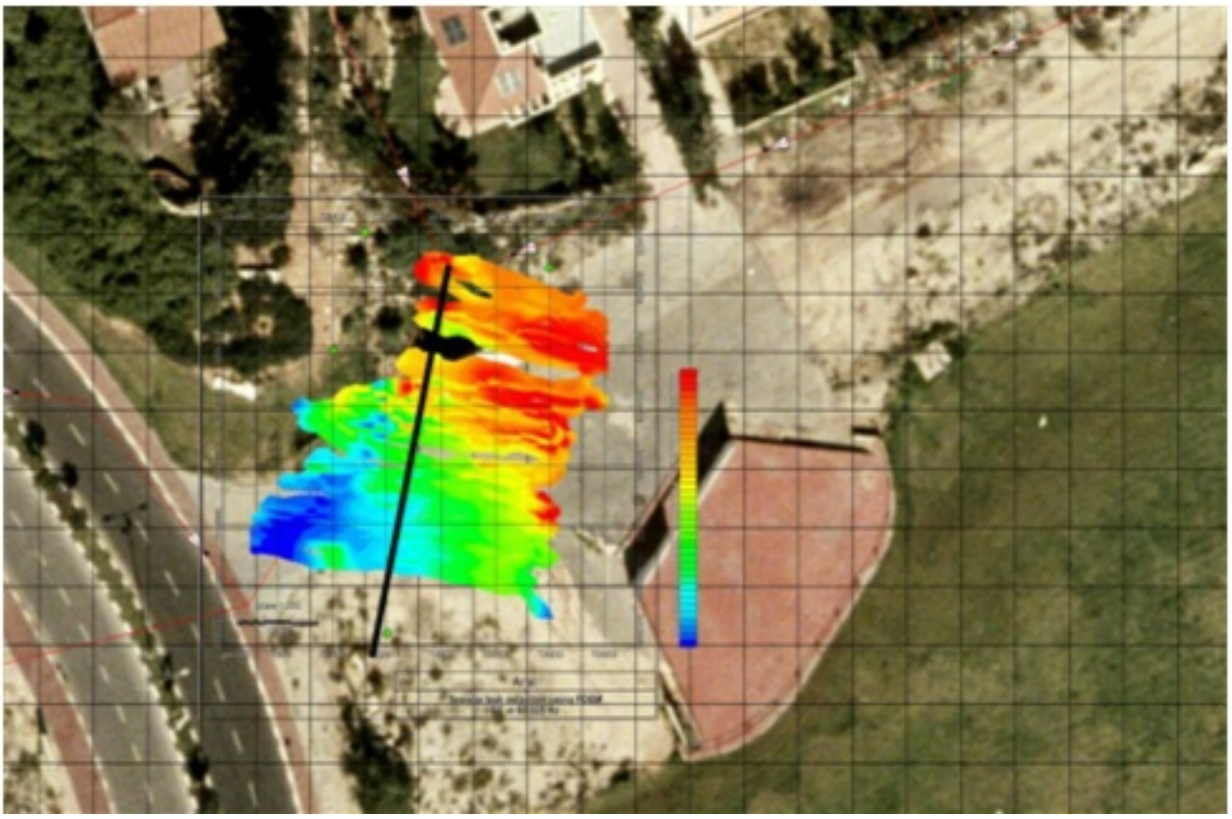

Figure 10. Map of the integrated electrical conductivity at 60,025 Hz before the start of the controlled leak at the western site (locations of the measurements are shown by the blue rectangle in Figure 8). The map is based on measurements performed with a GEM-2 FDEM sensor. The location of the sewer pipe is marked with a black line. Data were collected prior to the leak with dimensional scanning of approximately 30 m × 25 m. Lower conductivity (σ) values (11 mS/m) appear in blue-green in the southwestern corner of the area, while the highest conductivity appears in red-purple (55 mS/m) in the northeastern part of the map. These conductivity changes suggest anomalous subsurface moisture from the water pipe near the old stadium, as well as the accumulation of water from the slope, where there is a garden.

Figure 11 shows a pronounced increase in electrical conductivity of about 40 mS/m after 4 days of controlled leakage. The area has high conductivity because of changes in wetness due to a significant increase in liquid as a result of the sewage flow.

The results of the FDEM measurements conducted 10 days after the beginning of the controlled leak are presented in Figure 12. This picture may look similar to Figure 11 in terms of colors, but their intensity has increased due to an increase in the conductivity values to about 152 mS/m.

On the map in Figure 12, low visibility, reflecting low electrical conductivity, is shown in blue-green shades, high visibility in red-colored shades. Purple indicates sewer leakage on the background of the driest area, highlighting the differences in moisture. A wide area can be seen west of the pipe (black line in Figure 12) with relatively low electrical conductivity compared to the rest of the region. Northeast of the pipe, there is high electrical conductivity resulting from the spillover of sewage water.

http://dx.doi.org/10.5772/62156

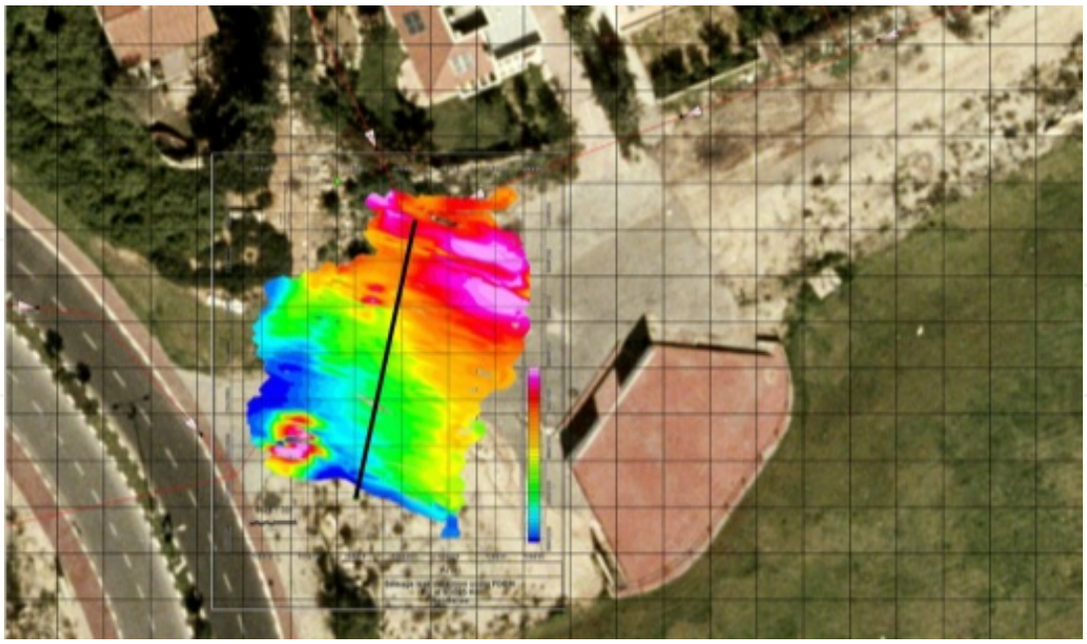

Figure 11. Map of the electrical conductivity at 60,025 Hz after about 4 days of leakage. Measurements were collected during the sewage leak, under wet conditions, with the GEM-2 sensor (locations of the measurements are shown by the blue rectangle in Figure 8). The location of the sewer pipe is marked with a black line. The highest conductivity value was about 95 mS/m. The significant increase in electrical conductivity is a result of the sewer liquids that were spilled during the 4 days of the controlled leak, in both the southwestern and northeastern sides of the area, probably due to a subsurface topography gradient.

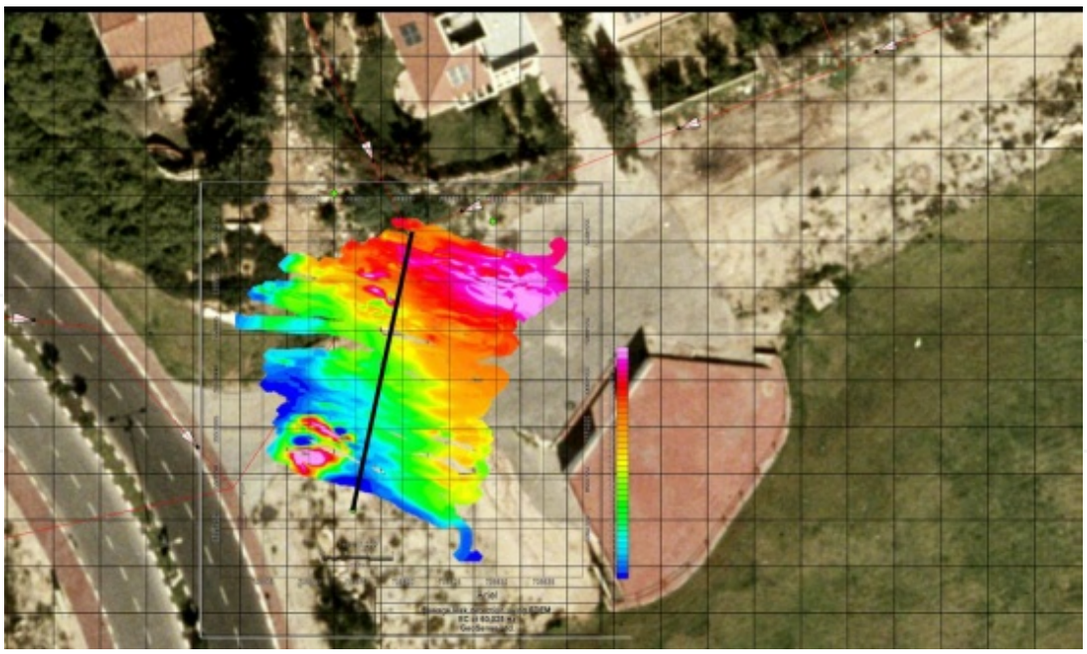

Figure 12. Map of integrated electrical conductivity at 60,025 Hz. Measurements were collected with the FDEM system, under wet conditions, after 10 days of controlled leakage (locations of the measurements are shown by the blue rectangle in Figure 8). Electrical conductivity ranged from 0 to 152 mS/m. Low conductivity is expressed in blue-green shades, high conductivity in purple-red colors.

Figure 13 shows maps made by FDEM monitoring of electrical conductivity at various frequencies in the first tested area. The maps are arranged, from left to right, at increasing frequencies and depth: the frequencies were 2,025 Hz, 4,725 Hz, 11,025 Hz, 25,725 Hz and 60,025 Hz, each frequency representing a 30 cm increase in depth. The low-visibility electrical conductivity is represented by blue-green hues, and the high-visibility electrical conductivity by red-purple hues. There were a few quantitative differences in the map scales.

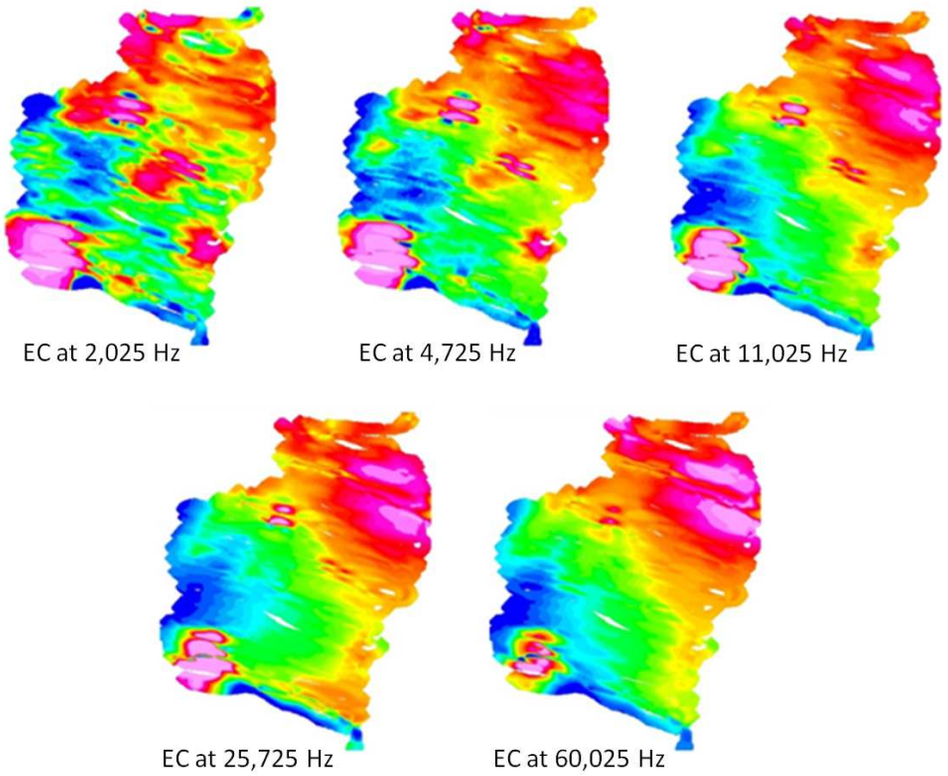

Figure 13. Maps made by FDEM monitoring of electrical conductivity at 2,025 Hz, 4,725 Hz, 11,025 Hz, 25,725 Hz and 60,025 Hz. The lower EC values are represented by blue-green hues, and the higher EC values by red-purple hues. There were a few quantitative differences between the maps' scales.

Four sections, two on each side of the sewer, were monitored by GPR and are shown in Figure 14. The distance between the main radar cross-sectional cuts was approximately 0.5 m. The radar sections shown in Figure 14 were collected with an antenna at a nominal frequency of 250 MHz over the location of the underground sewage pipe at the first (western) test site. The first cross-section was obtained before the leak started and reflects the typical dry state of the ground in May. An incision was made a few days after the initiation of the leak and shows a relatively wet subsoil. The right cross-section shows an incision made at a lower depth, 10 days after leak initiation, indicating a further increase in wetness. Similar data processing was carried out for the three cross-sections to highlight their differences.

http://dx.doi.org/10.5772/62156

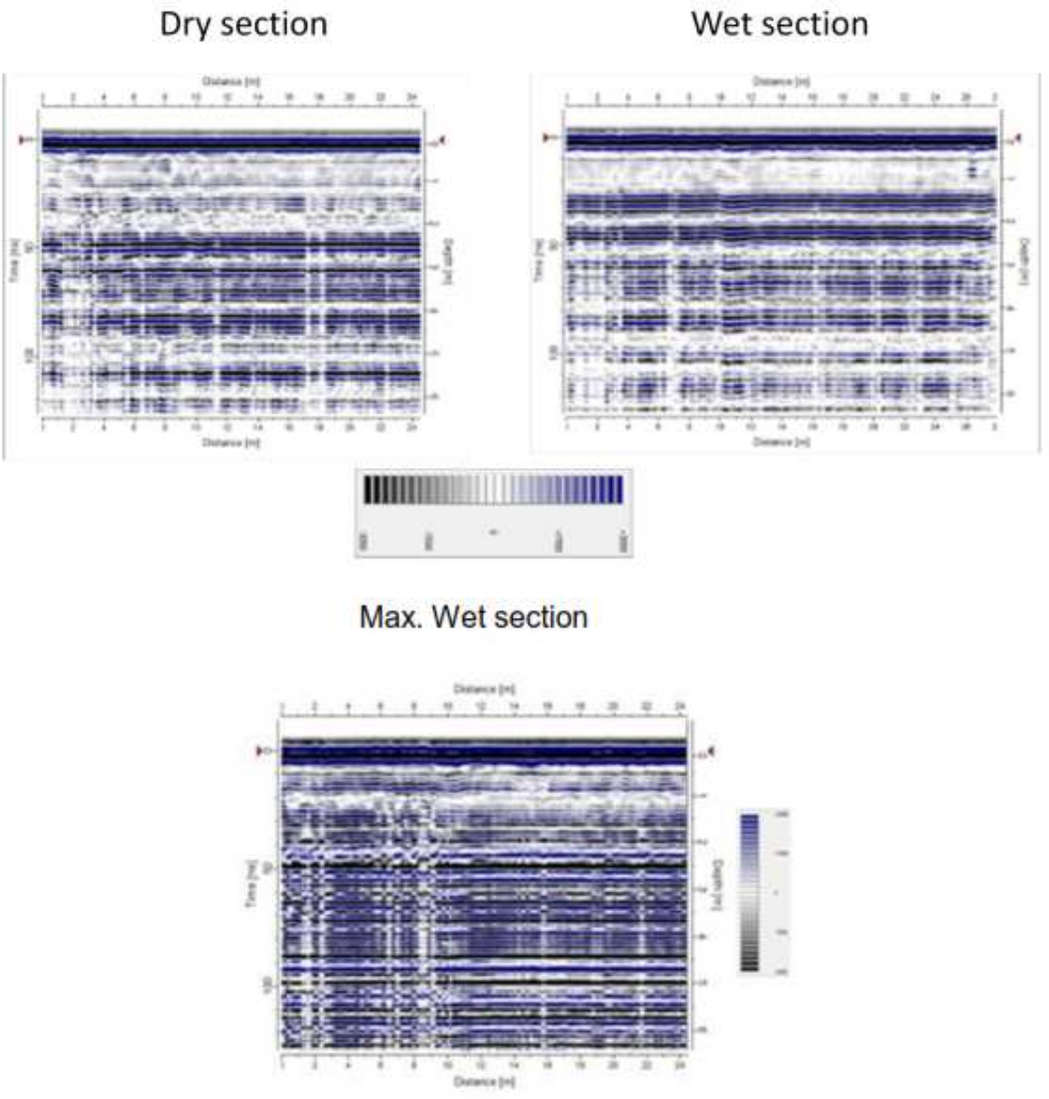

Figure 14. Soil moisture reflected by GPR cross-section (locations of the measurements are shown by the blue rectangle in Figure 8).

5. Modeling subsurface moisture content

Moisture content was computed on the basis of subsurface GPR and FDEM measurements and its spatial spread was obtained for calibration and wetness testing with water- and sewage-carrying pipelines. In these experiments, radar velocities were measured and dielectric constants were computed. Their correlations were used to measure the moisture content from data collected in the residential and industrial neighborhoods.

The computation of moisture content using GPR was based on the method developed by Basson [2] From the calibration measurements conducted at the end of May 2012, the average

subsurface EM wave velocity was 0.093 ± 0.001 m/ns. The calculated dielectric constant during this period was about 10.4. This value is low but not minimal, as minimal moisture content is typically found in the mid-to-late summer months (according to data from the Israel Meteorological Service, the rain that accumulated in the area in the months before the GPR measurements amounted to about 161 mm).

The velocity of EM waves in a substance is mainly a function of that substance's bulk dielectric properties and moisture content. When a substance is composed of a mixture of materials, the velocity is a function of their mixing ratios. In the case of a subsurface environment, we can treat the substance as a bulk property composed of soil, rock, minerals and organic materials mixed with air and water. When the rate of air increases, the velocity increases as well. However, when the moisture content increases, the average dielectric constant decreases as well and fro equation (6) it can be seen that the EM velocity (v) decreases as well.

The difference in the effective dielectric constant of "dry" and "wet" soils is mainly a function of the ratio between the air and water volumes, when the volumes are normalized according to equations (7) and (8). The maximal soil–water absorbency is a strong function of the effective porosity. For soils in the Ariel region, the effective porosity can vary from 40% to 60%. We used an average effective porosity of 50% in our computations. Therefore, the possible mixing ratios relative to the normalized volume are:

$$V_{\text{dry soil}} = 0.5\,V_{\text{tot}} \tag{9}$$

$$V_{\text{w}} + V_{\text{a}} = 0.5 V_{\text{tot}} \tag{10}$$

Since $k_{\text{dry soil}}$ is the effective dielectric constant measured using GPR imaging for a soil with residual moisture content and since $k_{\text{a}} = 1$:

$$k_{\text{top soil}} = 0.5 k_{\text{dry soil}} + 80 V_{\text{w}} + 0.5 - V_{\text{w}} \tag{11}$$

The radar wave velocity for “dry” soil at the surface will be measured and is expected to vary with the GPR and its value, $v_{\text{top soil}}$ ~ 0.07–0.14 m/ns. From Equation (1), this velocity range can reflect dielectric constant values of ~4.6–18.4 for $k_{\text{top soil}}$. For example, for maximal dielectric constant values of 5–14 for delicate quartz-based soils and for the presented computations, the moisture content in the surface can vary as $V_{\text{w top soil}}$ ~ 0.4%–2.1%. In the same way, we can investigate deeper soils where the moisture content is expected to be greater. The average radar wave velocity ($v_{\text{humid soil}}$) measured by the GPR at the calibration site in Ariel at the end of May is 0.093 m/ns. Using Equation (1), this velocity reflects a dielectric constant value ($k_{\text{humid soil}}$) of 10.406. The additional volume of water needed to increase the dielectric constant from 4.6 to 10.41 can be computed as:

$$\Delta k = 5.81 \tag{12}$$

http://dx.doi.org/10.5772/62156

$$\Delta k = 80\Delta V_{\mathrm{w}} \tag{13}$$

$$\Delta V_{w} = 7.26 \tag{14}$$

We develop a moisture content model using relative values of the moisture content (based on Equations (6–14)) causing an increase in electrical conductivity as measured by the FDEM. We had to consider the overall subsurface features, such as texture, density and effective porosity, as well as the content of salts in soils irrigated with brackish effluent water. The model results are presented in the graph in Figure 15.

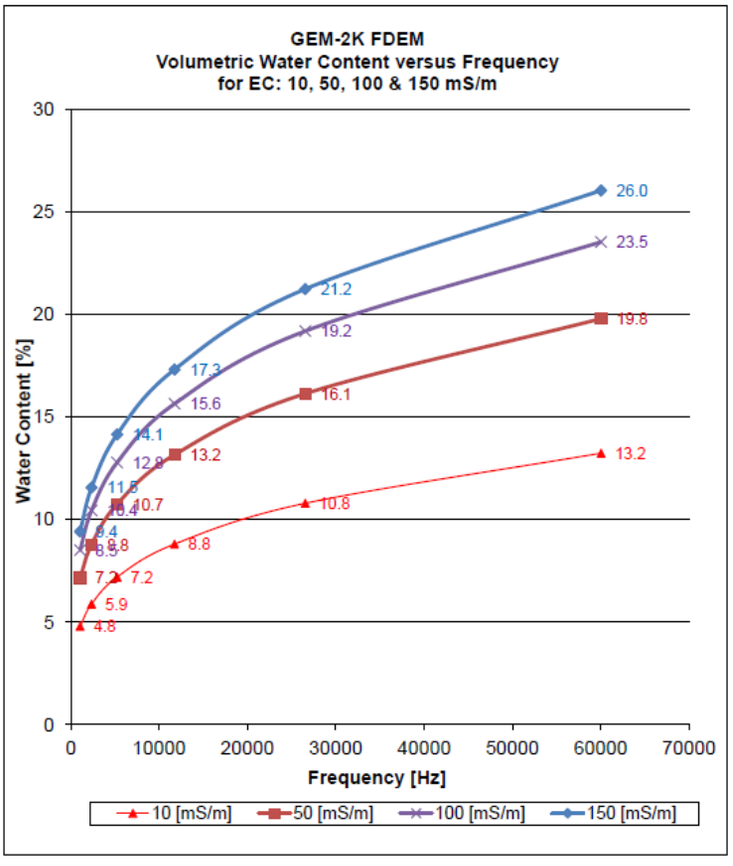

Figure 15. Volumetric moisture content calculated from measurements and from the FDEM model in the experimental zones in Ariel (accuracy ±10% of the measured value).

6. Discussion and conclusions

We introduced a combination of GPR and FDEM orthogonal methods to detect subsurface leaks from a sewage pipeline system. The rationale for this combination is to increase the

probability of detection, especially in complex urban environments and when the soil–rock setting can vary from relatively resistive to relatively conductive. The results of our study indicate that even minor leaks, such as the minor controlled leaks created in the experiment, and changes in the subsurface moisture content can be accurately detected. We could detect sewage leakage, as well as its progress. The combination of the two methods enabled not only the detection of the leak but also a qualitative assessment of its size. Factors affecting the ability to detect leaks were limited by the soil–rock conductivity, as well as the density of the terrain and subterrain systems and structures. The geophysical methods may detect sewage effluent flow paths as well as the contaminant in the soil.

The limestone and dolomite bedrock in the Ariel area is suitable for GPR mapping. The clarity of the GPR profile enabled analysis and interpretation of the physical data with good accuracy. We could detect sewage leakage, as well as its progress. The anomalous moisture of the leakage accumulating around the sewage pit in the southwest research area validated the efficiency of the methods.

Acknowledgements

The research was supported by the Israel water authority and by the Water Cooperation of Yuvalim. We would like to thank Mr. Omer Shamir from GeoSense for assistance with the data collection.

Author details

Goldshleger Naftaly[1,2*] and Basson Uri[3]

*Address all correspondence to: Goldshleger1@gmail.com

1 Civil Engineering Ariel University, Israel

2 Israel Ministry of Agriculture, Beit Dagan, Israel

3 Geosense Ltd., Even Yehuda, Israel

References

[1] Basson, U., and Ben-Avraham, Z., 1994. Subsurface spatial mapping of pollutants concentrations using ground penetrating radar. Proceedings of the 25th Annual Meeting of the Israel Society for Ecology and Environmental Quality Sciences, Tel-Aviv, Israel, 3–4 May 1994, p. 29.

[2] Basson, U., 1992. Mapping of Moisture Content and Structure of Unsaturated Sand Layers with Ground Penetrating Radar. M.Sc. thesis.Tel-Aviv University, Tel-Aviv, Israel.

[3] Basson, U., 2000. Imaging of Active Fault Zone in the Dead Sea Rift: Evrona Fault Zone as a Case Study. Ph.D. thesis. Tel-Aviv University, Tel-Aviv, Israel.

[4] Goldshleger, N., Mirlas, V., Ben-Dor, E., Eshel, M., and Basson, U., 2007. *Using Remote Sensing Methods for Improving the Management of Saline Affected Soils* ERSA, Conference Paris, France.

[5] Goldshleger, N., Livene, I., Chudnovsky, A., and Ben-Dor, E., 2012. Integrating passive and active remote sensing methods to assess soil salinity: a case study from Jezre'el Valley, Israel, Soil science 177(6), 392–401.

[6] Basson, U., 2007. Imaging and mapping subsurface infrastructures and buildings using GPR and FDEM electromagnetic methods. *Journal of Nondestructive News, Vol. 10, pp. 29-30*.

[7] Ben-Dor, E., Goldshleger, N., Eshel, M., Mirablis, V., and Basson, U., 2008.Combined active and passive remote sensing methods for assessing soil salinity. In: *Remote Sensing of Soil Salinization. Impact and Land Managemen* (G. Metternicht and A. Zinck, eds.), pp. 235–255. CRC Press, USA.

[8] Ben-Dor, E., Metternicht, G., Goldshleger, N., Eshel, M., Mirablis, V., and Basson, U., 2008. Review of remote sensing based methods to assess soil salinity. In: *Remote Sensing of Soil Salinization. Impact and Land Management* (G. Metternich and A. Zinck, eds.), pp. 39–60. CRC Press, USA.

[9] Ly, D.K., and Chui, T.F., 2012. Modeling sewage leakage to surrounding groundwater and storm water drains. *Water Science Technology* 66(12), 2659–2665.

[10] Ben-Dor, E., Heller, D. and A. Chudnovsky, 2008. 10. A novel method of classifying soil A A novel method of classifying soil profiles in the field using optical means Soil Science Society of American Journal, *72:1-13*.

[11] Klein, W.R., 1993. Acoustic leak detection. *American Society of Mechanical Engineers, Petroleum Division* 55, 57–61.

[12] Hough, J.E., 1988, Leak testing of pipelines uses pressure and acoustic velocity. *Oil and Gas Journal* 86, 35–41.

[13] Hunaidi, O., and Wang, A., 2004. Acoustic methods for locating leaks in municipal water pipe networks. *International Water Demand Management Conference, Dead Sea, Jordan, 30 May–3 Jun 2004*.

[14] Frischknecht, F.C., 1967. Fields about an oscillating magnetic dipole over a two-layer earth and application to ground and airborne electromagnetic surveys. *Quarterly of the Colorado School of Mines* 62, 326.

[15] Ward, S.H., 1967. Electromagnetic theory for geophysical applications. In: *Mining Geophysics* (S.H. Ward, ed.), pp. 13–196. Society of Exploration Geophysicists, Theory, USGS.

[16] Ward, S.H., and Hohmann, G.W., 1988. Electromagnetic theory for geophysical applications. In: *Electromagnetic Methods in Applied Geophysics* (M.N. Nabighian, ed.), pp. 130–311. Society of Exploration Geophysics, Theory, Tulsa, Oklahoma.

[17] Won, I.J., and Huang, H., 2004. Magnetometers and electro magnetometers. *The Leading Edge* 23(5), 448–451.

[18] Huang, H., and Won, I.J., 2003. Real-time resistivity sounding using hand-held electromagnetic sensor. *Geophysics* 68(4), 1224–1231.

[19] Davis, J.L., and Annan A.P., 1986. High resolution sounding using ground probing radar. *Geoscience Canada* 3: 205–208.

[20] Davis, J.L., and Annan, A.P., 1989. Ground penetrating radar for high resolution mapping of soil and rock stratigraphy. *Geophysical Prospecting* 37: 531–551.

[21] Dan, Y., and Raz, Z., 1970. *Soil Association Map of Israel*. Volcani Institute for Agriculture Research, Israel (in Hebrew).

[22] Soil Survey Staff, 1975. *Soil Taxonomy: A Basic System of Soil Classification for Making and Interpreting Soil Surveys.* US Department of Agriculture, Handbook 436, pp. 754.